Original Article PROGRESS in MEDICAL PHYSICS Vol. 27, No. 1, March, 2016
http://dx.doi.org/10.14316/pmp.2016.27.1.1

Compressed-sensing (CS)-based Image Deblurring Scheme with a Total Variation Regularization Penalty for Improving Image Characteristics in Digital Tomosynthesis (DTS)

Uikyu Je, Kyuseok Kim, Hyosung Cho, Guna Kim, Soyoung Park, Hyunwoo Lim, Chulkyu Park, Yeonok Park

Department of Radiation Convergence Engineering and *i*TOMO Research Group, Yonsei University, Wonju, Korea

In this work, we considered a compressed-sensing (CS)-based image deblurring scheme with a total-variation (TV) regularization penalty for improving image characteristics in digital tomosynthesis (DTS). We implemented the proposed image deblurring algorithm and performed a systematic simulation to demonstrate its viability. We also performed an experiment by using a table-top setup which consists of an x-ray tube operated at 90 kV_p, 6 mAs and a CMOS-type flat-panel detector having a 198-μm pixel resolution. In the both simulation and experiment, 51 projection images were taken with a tomographic angle range of θ=60° and an angle step of $\Delta\theta$=1.2° and then deblurred by using the proposed deblurring algorithm before performing the common filtered-backprojection (FBP)-based DTS reconstruction. According to our results, the image sharpness of the recovered x-ray images and the reconstructed DTS images were significantly improved and the cross-plane spatial resolution in DTS was also improved by a factor of about 1.4. Thus the proposed deblurring scheme appears to be effective for the blurring problems in both conventional radiography and DTS and is applicable to improve the present image characteristics.

Key Words: Compressed-sensing (CS), Digital tomosynthesis (DTS), Deblurring, Total variation (TV)

Introduction

Digital tomosynthesis (DTS) has been popularly used as a multiplanar imaging modality in medical and industrial x-ray imaging applications. It is a geometric tomography by a limited-angle scan to provide cross-sectional images of the scanned object with a moderate cross-plane resolution.[1,2] However, although it provides some of the tomographic benefits of computed tomography (CT) at a reduced imaging dose and time, the image characteristics is relatively inferior mainly due to the blur artifacts originated from incomplete data sampling for a limited angular range and also aspects inherent to imaging system such as finite focal spot of the x-ray source, detector resolution, system noise, *etc*. Thus the recovery of x-ray images from their blurred and noisy version, collectively referred to as *image deblurring*, has been extensively studied during the past decades.

In this work, we considered a compressed-sensing (CS)-based deconvolution method for image deblurring of high accuracy in DTS. Here the CS is the state-of-the-art mathematical theory for solving the inverse problems, which exploits the sparsity of the image with substantially high accuracy.[3] We implemented the proposed deblurring algorithm and performed a systematic simulation and experiment to demonstrate its viability for improving the image characteristics. In the following sections, we briefly describe the implementation of the proposed deblurring algorithm, the simulation and experimental

This work was supported by the Radiation Technology Development Program of the National Research Foundation (NRF) funded by the Korea Ministry of Science, ICT & Future Planning under Contract No. 2015-51-0284.
Received 10 March 2016, Revised 25 March 2016, Accepted 28 March 2016
Correspondence: Hyosung Cho (hscho1@yonsei.ac.kr)
Tel: 82-33-761-9660, Fax: 82-33-761-9664

setup, and we present the obtained results.

Materials and Methods

1. CS-based image deblurring scheme

Most of the previous image deblurring methods are based on the standard image degradation modeling in which the observed image, $g(x,y)$, is formed by convolving the original (or *exact*) image, $f(x,y)$, by the shift-invariant point-spread function (PSF) of the system, $psf(x,y)$, followed by adding white Gaussian noise, $n(x,y)$:

$$g(x,y)=f(x,y)\otimes\otimes psf(x,y)+n(x,y) \quad (1)$$

where the operator $\otimes\otimes$ represents two-dimensional (2D) convolution. Thus the degraded image can be restored by the deconvolution method, provided that PSF is known.[4] The PSF is the 2D image profile of a point object which describes the amount of blurring by the imaging system. Numerous deconvolution methods such as Wiener filtering, least-squares filtering, wavelet-based algorithms, *etc*., have already been established in the literature.[5,6] However, as indicated in (1), one critical difficulty in the deconvolution problem is associated with the presence of noise in the blurred image, which results in imperfect deconvolution.

In this work, as a highly accurate deconvolution method, we employed a CS-based image deblurring scheme incorporated with the total-variation (TV) regularization penalty. Here the TV is the l^1-norm of the gradient image and is often used as an effective regularization penalty in many image recovery problems such as denoising, deblurring, and inpainting due to its ability to preserve image edges.[7] In the CS-based deblurring scheme, the original image f is recovered normally by minimizing the following objective function, $\phi(f)$, as the solution to a convex optimization problem, f^*, described in (2), assuming that the negligible components of the gradient image are nearly zeros:

$$\phi(f)=\frac{1}{2}\|f\otimes\otimes psf-g\|_2^2+\alpha\|f\|_{TV},$$

$$f^*=\arg\min_{f\in Q}\ \phi(f) \quad (2)$$

where $1/2\|f\otimes\otimes psf-g\|_2^2$ is the fidelity term, $\|f\|_{TV}$ is the TV regularization penalty term, α is the parameter that balances the two terms and is chosen so that signal-to-noise ratio is maximized (e.g., α=0.04 was used in this work), and Q is the set of feasible f. The convex optimization problem described in (2) can be solved approximately, but efficiently, by using the accelerated gradient-projection-Barzilai-Borwein (GPBB) method.[8]

Fig. 1 shows the schematic illustration of a typical DTS geometry in which an x-ray source and a flat-panel detector move together in an arc around the pivot during the projection data acquisition. Fig. 2 shows the simplified flowchart of the CS-based deblurring scheme in DTS implemented in this study. Briefly to describe, firstly, the projection images of an imaged

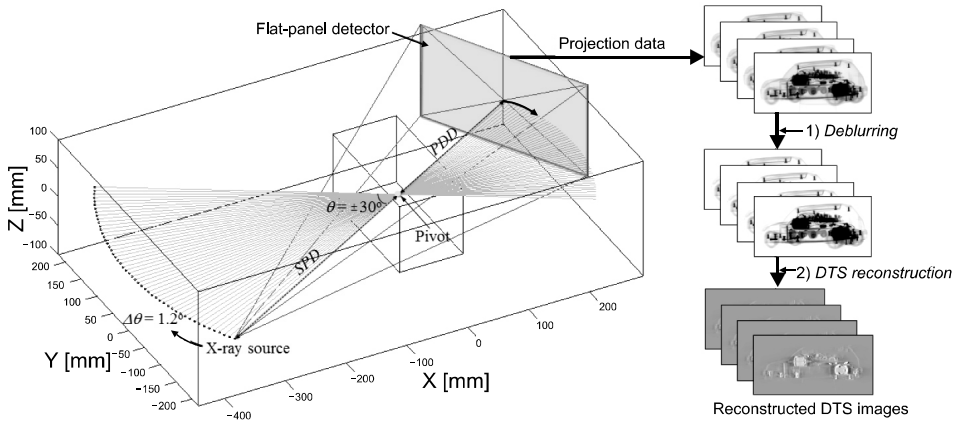

Fig. 1. Schematic illustration of a typical DTS geometry in which an x-ray source and a flat-panel detector move together in an arc around the pivot during the projection data acquisition.

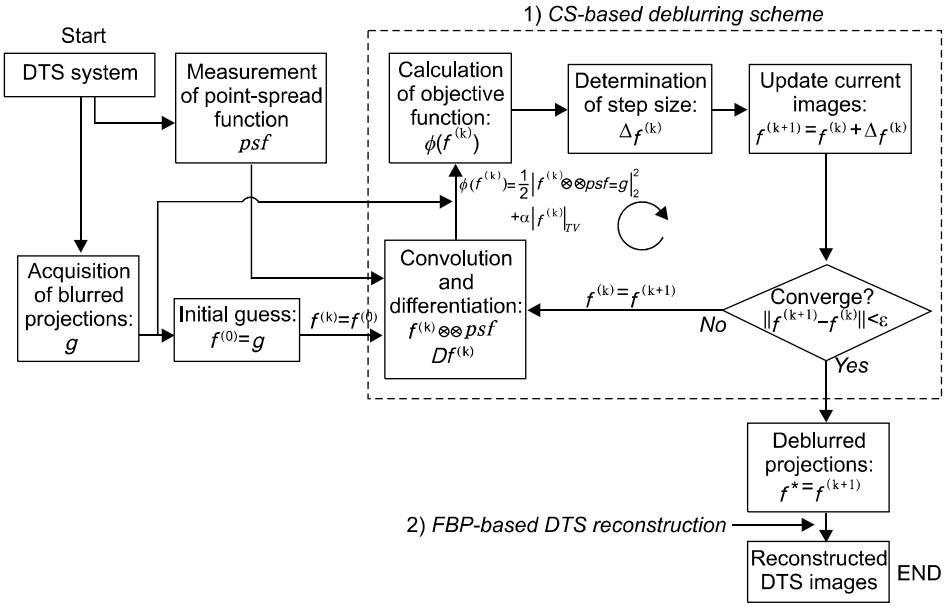

Fig. 2. Simplified flowchart of the CS-based deblurring scheme in DTS. The acquired projection images are deblurred through the CS-based scheme before performing the common FBP-based DTS reconstruction.

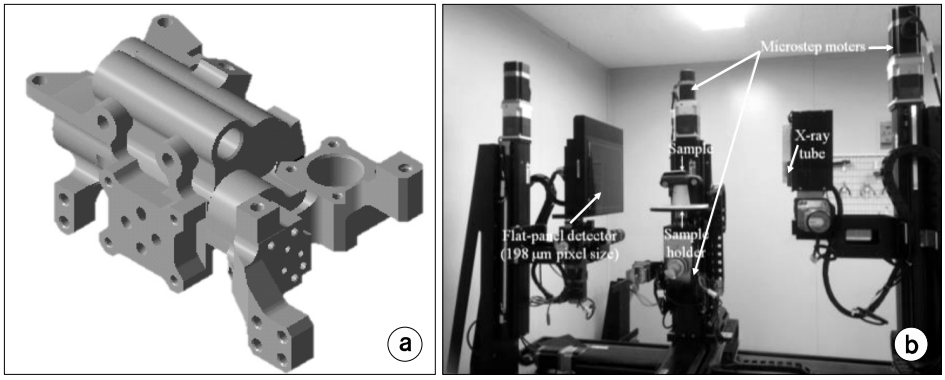

Fig. 3. (a) 3D numerical phantom of a pump casting used in the simulation and (b) the table-top setup that we established for the experiment.

object are acquired from the imaging system and then they are assumed as the initial gauss $f^{(0)}$ before applying the CS-based framework as the current updated images $f^{(k)}$. By using the $f^{(k)}$ and the *psf* measured separately, the objective function $\phi(f)$ is computed to determine an optimal step size $\Delta f^{(k)}$ for the next updated images $f^{(k+1)}$. The images f are successively updated until the mismatch between the current and the next updated images converges to a specified tolerance ε before performing the common filtered-backprojection (FBP)-based DTS reconstruction. More detailed descriptions of the FBP-based DTS reconstruction can be found in our previous paper.[9)]

2. Simulation and experimental setup

Based on the above descriptions, we implemented an effective CS-based deblurring algorithm by using the Matlab™ (ver. 8.3) programming language and performed a systematic simulation and experiment to investigate the image characteristics. Fig. 3 shows (a) the 3D numerical phantom of a pump casting used in the simulation and (b) the table-top setup that we established for the experiment. The table-top setup mainly consists of an x-ray tube whose operating conditions are 90 kV_p and 6 mA, a CMOS-type flat-panel detector having a 198-μm pixel resolution, and a sample holder. In the both simulation and the experiment, 51 projection images were taken with a tomographic angle range of $\theta=60^o$ and an angle step of $\Delta\theta=1.2^o$ and then deblurred by using the CS-based deblurring algorithm before performing the common FBP-based DTS reconstruction.

Fig. 4 shows (a) the measured 1D line-spread function (LSF) curve with a Gaussian fit (standard deviation σ=0.358 mm), and (b) the resultant 2D blur kernel having a filter size of 15×15. Here we used a slit camera (Pro-Project Corp., 05-101) having a 10-μm width for measuring the 1D LSF. The same blur kernel was used in the both simulation and the experiment. The resultant DTS images were reconstructed with a voxel size of 0.198 mm×0.198 mm×0.198 mm and voxel dimensions of 426×240×198 for the simulation and 532×1,064×582 for the experiment. Although the implemented algorithm has not yet been accelerated by the graphics processing unit (GPU), the total time for image deblurring and DTS reconstruction was less than 20 minutes on a normal workstation. Detailed geometrical and reconstruction parameters used in the simulation and experiment are listed in Table 1.

Results and Discussion

Fig. 5 shows (a) some examples of the blurred (*left*) and the

Table 1. Geometrical and reconstruction parameters used in the simulation and experiment.

Parameter	Dimension
Source-to-pivot distance (*SPD*)	442.8 mm
Pivot-to-detector distance (*PDD*)	288.6 mm
Tomographic angle range (θ)	60°
Angle step ($\Delta\theta$)	1.2°
Pixel size	0.198 mm
Voxel size	0.198 mm
Test object (dimension)	Pump casting (426×240×198), toy car (532×1,064×582)
Deblurring algorithm	CS-based
DTS algorithm	FBP-based

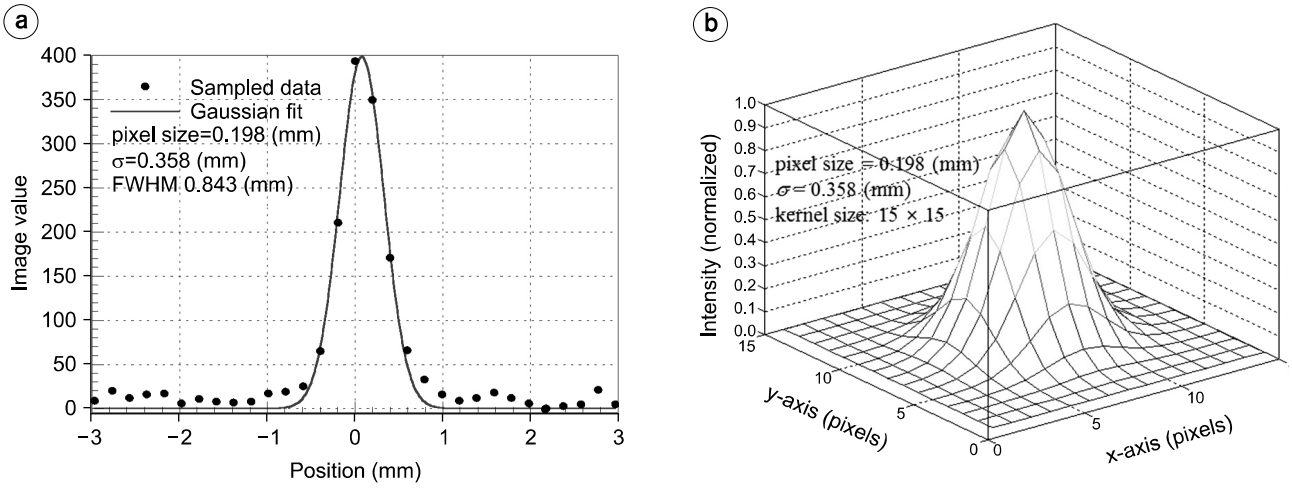

Fig. 4. (a) Measured 1D LSF curve with a Gaussian fit, and (b) the resultant 2D blur kernel having a filter size of 15×15. The same blur kernel was used in the both simulation and the experiment.

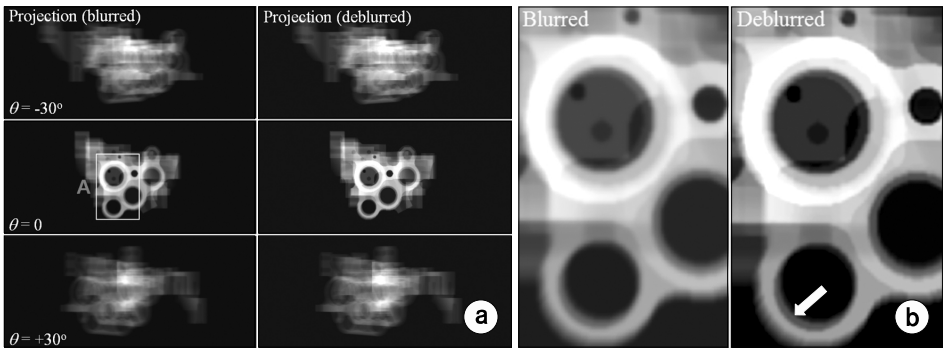

Fig. 5. (a) Some examples of the blurred (*left*) and the deblurred (*right*) projection images of the pump casting and (b) their enlarged images indicated by the box *A* in (a). Only three projection images (*i.e.*, for $\theta = -30°$, 0, and $+30°$) out of the 51 are indicated for simplicity).

deblurred (*right*) projection images of the pump casting, and (b) their enlarged images indicated by the box *A* in (a). Only three projection images (*i.e.*, for $\theta = -30^{o}$, 0, and $+30^{o}$) out of the 51 are indicated for simplicity. Note that the deblurred projection images are quite visible, compared to the blurred images, which demonstrates the viability of the proposed scheme for image deblurring in x-ray imaging. Fig. 6 shows some examples of the reconstructed DTS images of the pump casting from the front side (*top*) to the rear side (*bottom*) for no blurring, blurring, and deblurring cases. Here only 4 slices out of the 426 are indicated for simplicity. The phantom slice images (*the leftmost*) are also indicated as the reference. Fig. 7 shows the enlarged DTS images indicated by the box *A* in Fig. 6. Also note that how the structures of the pump casting in the

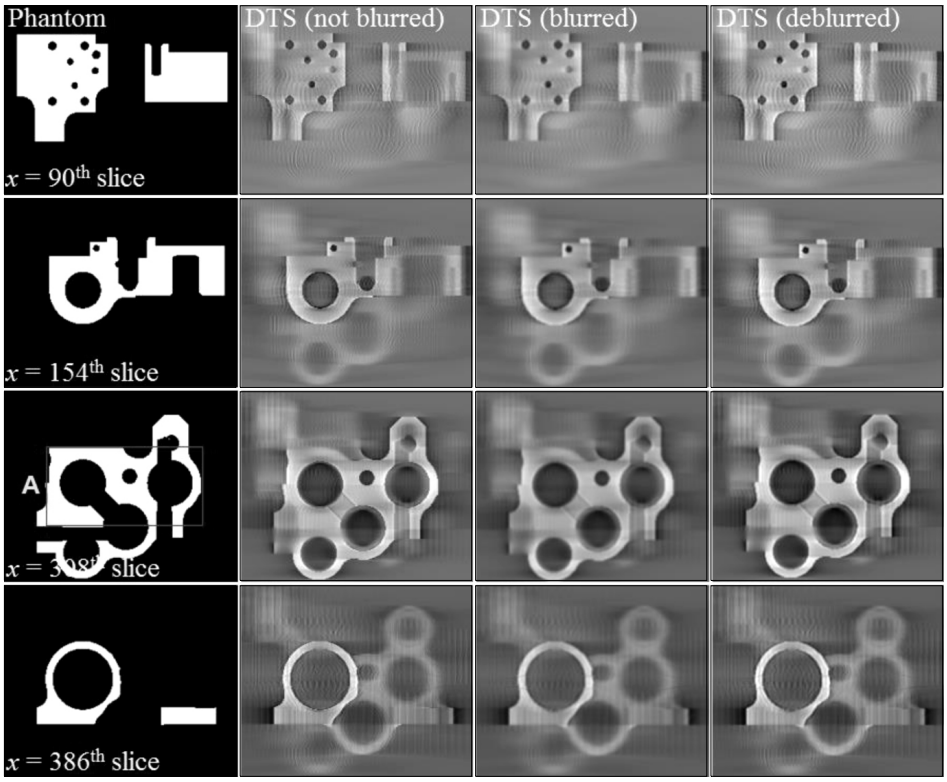

Fig. 6. Some examples of the reconstructed DTS images of the pump casting from the front side (*top*) to the rear side (*bottom*) for no blurring, blurring, and deblurring cases. Only 4 slices out of the 426 are indicated for simplicity. The phantom slice images (*the leftmost*) are also indicated as the reference.

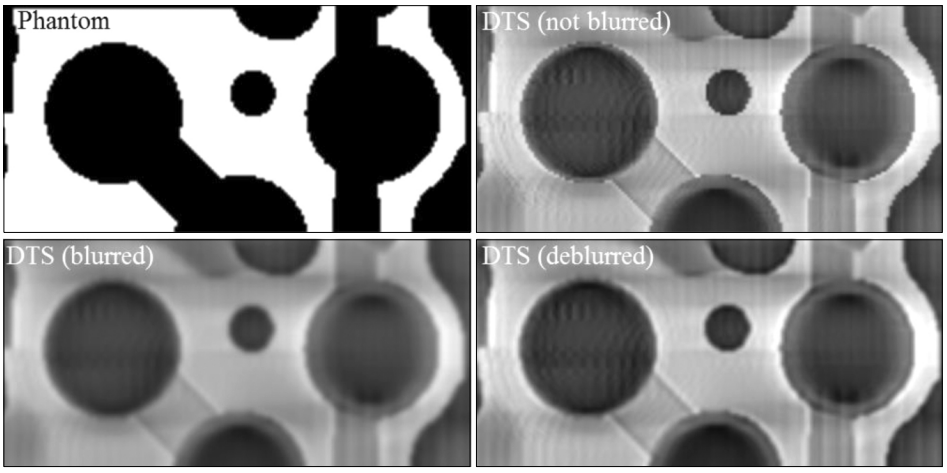

Fig. 7. The enlarged DTS images indicated by the box *A* in Fig. 6 for no blurring, blurring, and deblurring cases. The phantom slice image (*upper left*) is also indicated as the reference.

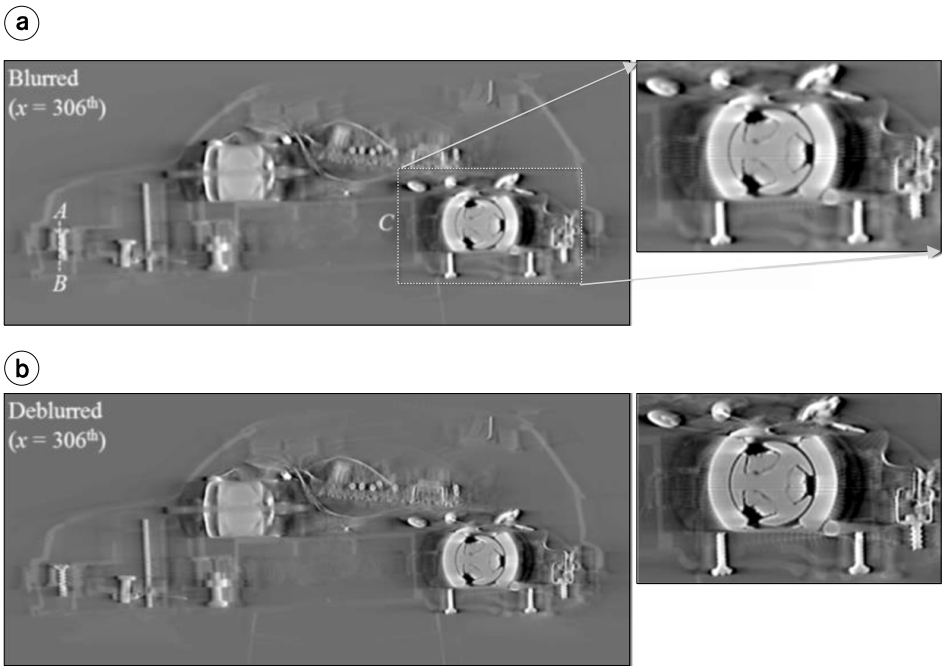

Fig. 8. An example of the reconstructed DTS images of the toy car (*i.e.,* for x=306th slice) for (a) blurring and (b) deblurring cases.

deblurred DTS image is quite visible, demonstrating the viability of the proposed scheme for image deblurring in DTS as well. Fig. 8 shows an example of the reconstructed DTS images of the toy car (*i.e.*, for x=306th slice) for (a) blurring and (b) deblurring cases, which is similar to the simulation result.

One thing that should be addressed is that the cross-plane resolution in DTS is usually inferior to that in CT due to its limited-angle scan, which produces relatively worse tomographic features. The cross-plane resolution in tomography is often described by the slice-sensitivity profile (SSP). Similar to the in-plane resolution, the SSP describes the system response to a Dirac delta function $\delta(x)$ in x (*i.e.*, along the depth direction of the imaging volume). In many cases, the SSP curve itself is replaced by the full-width at half-maximum (FWHM). In order to evaluate the SSP characteristic, we performed the same DTS reconstruction by using a small thin-square (1×5×5) phantom which is located at the mid-plane (*i.e.*, x=51st slice) of the imaging volume. Fig. 9 shows the measured SSP curves along the x-axis from the reconstructed DTS images of the small thin-square phantom. Here the intensity profile of the phantom in x is also indicated as the reference. The measured FWHM value for the deblurred DTS images was about 1.23 mm, about 1.4 times smaller than that for the blurred images, indicating that the proposed deblurring scheme is also effective

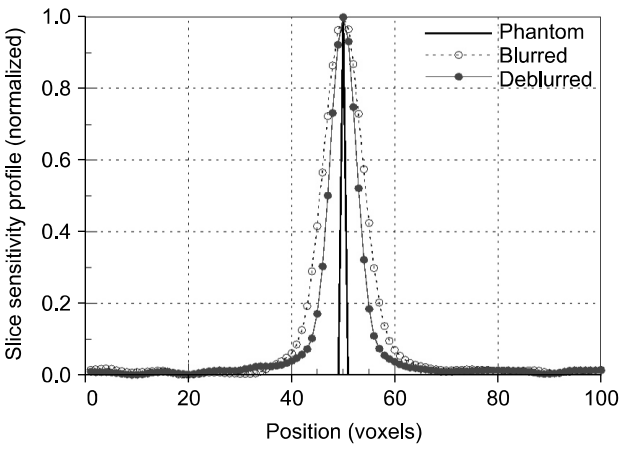

Fig. 9. The measured SSP curves along the x-axis from the reconstructed DTS images of the small thin-square phantom. Here the intensity profile of the phantom in x is also indicated as the reference.

for improving the cross-plane resolution in DTS.

Consequently, according to our simulation and experimental results, the CS-based deblurring scheme seems to be effective for improving the image characteristics in DTS as well as in x-ray imaging.

Conclusion

In this work, as an effective image recovering method, we proposed a CS-based image deblurring scheme incorporated with the TV regularization penalty for improving the present image characteristics in DTS. Our results indicate that the image sharpness of the recovered x-ray images and the reconstructed DTS images were significantly improved and the cross-plane spatial resolution in DTS was also improved by a factor of about 1.4, which demonstrates the viability of the proposed scheme for image deblurring of high accuracy in DTS. However, during the CS-based iterative procedure, each iteration loop requires one forward-projecting and one backward-projecting operations, taking a much longer reconstruction time, which is the primary computational bottleneck especially in 3D reconstruction. Thus the graphics processing unit (GPU) should be implemented in the proposed algorithm to accelerate the reconstruction processing in the future.

References

1. J. Dobbins and D. Godfrey: Digital x-ray tomosynthesis: current state of the art and clinical potential. Phys. Med. Biol. 48(19): R65-106 (2003)
2. F. Xu, L. Helfen, T. Baumbach, and H. Suhonen: Comparison of image quality in computed laminography and tomography. Opt. Express 20(2): 794-806 (2012)
3. K. Choi, J. Wang, L. Zhu, T. S. Suh, S. Boyd, and L. Xing: Compressed sensing based cone-beam computed tomography reconstruction with a first-order method. Med. Phys. (37): 5113-5125 (2010)
4. H. Xu, T. Huang, X. Lv, and J. Liu: The Implementation of LSMR in Image Deblurring. Appl. Math. Inf. 8(6): 3041-3048 (2014)
5. M. Figueiredo and R. Nowak: An EM algorithm for wavelet-based image restoration. IEEE Trans. Image Process. 12: 906-916 (2003)
6. X. Li: Fine-granularity and spatially-adaptive regularization for projection-based image deblurring. IEEE Trans. Image Process. 20: 971-983 (2011)
7. S. Babacan, R. Molina, and A. Katsaggelos: Parameter estimation in TV image restoration using variational distribution approximation. IEEE Trans. Image Process. 17(3): 326-339 (2008)
8. J. Park, B. Y. Song, J. S. Kim, et al.: Fast compressed sensing-based CBCT reconstruction using Barzilai-Borwein formulation for application to on-line IGRT. Med. Phys. 39(3): 1207-1217 (2012)
9. J. E. Oh, H. S. Cho, D. S. Kim, S. I. Choi, and U. K. Je: Application of digital tomosynthesis (DTS) of optimal deblurring filters for dental x-ray imaging. J of the Korean Phys. Soc. 60(6): 1161-1166 (2012)

디지털 단층합성 X-선 영상의 화질개선을 위한 TV-압축센싱 기반 영상복원기법 연구

연세대학교 방사선융합공학대학원, *i*TOMO연구팀

제의규 · 김규석 · 조효성 · 김건아 · 박소영 · 임현우 · 박철규 · 박연옥

본 연구에서는 디지털 단층합성 엑스선 영상의 화질특성을 개선하기 위해 TV-압축센싱 기반 영상복원 기법을 제안한다. 제안된 영상복원 기법의 유효성을 검증하기 위해 우선 관련 영상복원 알고리즘을 구현하였으며, 이를 이용하여 관련 시뮬레이션 및 실험을 함께 수행하였다. 실험을 위해 일반 x-선관(90 kV_p, 6 mAs), CMOS형 평판형 검출기(198 μm 픽셀크기)로 구성된 실험장치를 구성하였으며, 제한된 각도 60°도에서 2° 간격으로 총 51장의 투상영상을 획득하고 제안된 알고리즘으로 영상복원을 수행한 후 필터링 역투사법(FBP)을 사용하여 디지털 단층합성 영상을 구현하였다. 본 연구에서 수행된 결과에 의하면, 제안된 영상복원 기법은 일반 엑스선 영상 및 디지털 단층합성 영상의 흐린 영상화질을 선명하게 개선하고 또한 디지털 단층합성 영상의 깊이 분해능을 향상시키는 이점이 있음을 확인함으로써 기존 디지털 단층합성 영상의 화질을 크게 개선할 수 있을 것으로 전망된다.

중심단어: 압축센싱, 디지털 단층합성법, 영상흐림 제거, 총 변량